Multichannel and multicolour infrared thermography in Tore Supra

R. Reichle[1], C. Pocheau[1], C. Balorin[1], E. Delchambre[1,2], C. Desgrange[1], D. Guilhem[1], P. Messina[1], H. Roche[1]

[1] *Association EURATOM-CEA, CEA/DSM/DRFC, CEA-Cadarache, 13108 St. Paul-lez-Durance, France*

[2] *present address: EURATOM/UKAEA Fusion Association, Culham Science Centre, Abingdon OX14 3DB, UK*

An imaging spectrometer using a sapphire prism as dispersing element has been conceived at Tore Supra for the spectral range of 1 - 4 µm. It measures simultaneously at various wavelengths the temperature on distributed high heat-flux elements under plasma impact with 36 optical fibres, 4 of which are ZrF_4 fibres. It employs an InSb focal plane array detector (256*320 pixels) behind a silicon filter and a ZnS window yielding a dynamic range of 200 to 1500°C with 20 ms temporal resolution. The fibre transmission and the spatial variation of gain and background of the camera are calibrated using a light source with integrating sphere. With a black body source one determines the non linearity of the average gain and controls its stability during operation. The spectral dispersion of about 30 nm/pixel is determined with interference filters and controlled with a spectral lamp. The measurements at various wavelengths allow to determine the temperature distribution in the field of view.

1. Introduction

Thermography was proposed [1] and is being implemented [2] as the measuring method for the real time safety system to protect the new limiter of Tore Supra [3] against excessive heat-fluxes. Here we concentrate on the optical fibre system that is pointed towards the neutraliser plates, which are 12 target plates intercepting the scrape off layer plasma 50 mm outside the last closed magnetic flux surface below the limiter. Critical power fluxes were expected to correspond to surfaces temperatures of 1000-1300°C[1] defining the most important working range of the diagnostic. For physics studies the measurements should be usable from about 150°C, the usual vessel temperature. Preceding studies [7, 8] had shown that short wavelength measurements (0.9 – 1.6 µm) yield often higher temperatures than long wavelength (4.5 µm) measurements[2]. This has led to the conclusion to extend the measurement range beyond the near infrared range accessible with silica fibres transparent up to 2 µm up to the mid infrared range with ZrF_4 fibres transparent up to 4 µm. Tore Supra decided to use 4 ZrF_4 fibres (Verre Fluoré, France) and 32 silica fibres (Oxford Electronics, UK) to look with 12 individual periscopes each equipped with 3 fibres at each of the neutralisers and to pass the output of all these fibres through a dispersing sapphire prism onto a common 2 dimensional detector array. The principle and first results have been shown [2, 6]. This contribution gives the technical details on the apparatus, calibration and data-treatment and indications on the potential of determining a temperature distribution on a target from a measured luminance distribution.

2. Experimental arrangement

The in vessel installations of the periscopes, the arrangement of the lines of sight, the path of the fibres between the periscopes and the and the resulting image on the detector are described in [2 (fig. 6, 7c, 9, 10, 11)]. The fibre lengths between the measuring point and the detector vary from 6 to 9 m for the ZrF_4 fibres and from 6 to 12 m for the silica fibres. Fig. 1 shows the layout the dispersive system. The fibres are assembled in three concentrators A, B and C. A and B contain 21 near infrared (NIR) grade silica fibres with 0.3 mm core diameter at a pitch of 1 mm. C are ZrF_4 fibres with a core diameter of 0.2 mm at a pitch of 0.9 mm. 36 of the fibres are connected to the periscopes in the tokamak. Of the remaining fibres one is usually

[1] Higher temperatures at lower fluxes are actually observed in regions covered with redeposited and weakly attached carbon films [4, 5, 6].

[2] A nonhomogeneous target temperature distribution including small hot spot areas is meanwhile presumed to be the reason for this behaviour [9, 6, 10].

connected to a black body source at 400°C and two other ones to a Hg-Ar lamp. Lens 1 and lens 2 comprise two converging CaF_2 elements and a diverging Al_20_3 element. Lens 1 has a focal length of 150 mm (aperture F/6), lens 2 has 50mm (F/2.5), yielding a magnification of 0.33 for the projection of the fibres onto the detector chip. The prism is made of Al_20_3. Its height is 40 mm, its sides are 50 mm and the angle is 45° ± 0.5°. Between the lens 2 and the detector chip are a Si filter at room-temperature, a ZnS window and the cold aperture of the camera. The Si filter is a highpass filter for wavelengths above 1.04 µm. The detector chip has a size of 320*256 pixels with a pixel size of 30*30 µm. An integrating sphere of 10 cm diameter with an exit hole of 2.54 cm diameter can be imaged via the condenser lens 3 and a sliding mirror directly onto the camera to give a homogeneous illumination. This is either a sphere with a halogen lamp source or a sphere with a golden coating and an infrared filament source. Lens 3 consists of 2 planconvex CaF_2 elements, the flat faces of which are oriented towards the sphere with a distance of 3 mm between them. Their diameter is 50.8 mm and the focal length of each is 150 mm. The most commonly used mode of operation of the camera is that the camera runs internally at a frame rate of 150 Hz cyclically alternating the three (nominal) exposure times 1000 µs, 200 µs and 50 µs. Each frame is taken with 14 bits resolution. Values that exceed the value 13000 in a long exposure time are replaced by values at the next shorter exposure time (after 2^{14} has been added to that value for each switch of exposure time) in order to give the widest possible dynamic range. The outgoing frames have a rate of 50 Hz and are coded on 16 bits.

3. Calibration

The first step in the calibration chain is to normalise the gain and the offset variations of the focal plane array detector. This is done for each exposure time by illuminating the detector homogeneously at two illumination levels at about 10% and 90% of the maximum value with the integrating sphere via the sliding mirror. From the two measurements one can determine in an iterative process for each pixel gain and offset (background) and whether the pixel falls outside the specifications. One finds that the gain correction necessary corresponds well to the theoretical intensity decay towards the corners of the focal plane array as described by equation 1.

$$E(\Theta) = E_0 \cos^4(\Theta) \qquad (1)$$

E_0 represents the illumination in the centre of the detector, Θ represents the angle between the line connecting the centre of the aperture in front of the detector with the centre of the detector and the line from the centre of the aperture to the point of interest on the detector. The offset is rather flat over the field of view. It is positive for the smallest exposure times and rises linearly for exposure times larger the 100 µs to a value that saturates the measurement range at an exposure time of 2000µs.

The second step in the calibration chain is the determination of the dispersion function (fig. 2) of the prism. This is done with 7 interference filters of a width of 60 ± 10nm that can be inserted between the fibre concentrator and lens 1. The Hg-Ar lamp illuminating a fibre in group C and a fibre in group A allows to control the long term stability of the determined dispersion function during operation. Testing all fibres this way one finds the distorsion in the system. For the fibres in concentrator C this is negligible. For the fibres B it is also negligible for the 10 central fibres and amounts to 1.2 pixels for the extremes. For the concentrator A a clear parabolic distorsion is found reaching 4.5 pixel at the extremes. The vertical channel separation is 9-10 pixel. The vertical spread of the signal is aproximatively gaussian with a full width at half maximum of 3-5 channels. [2, fig. 10]. The horizontal (spectral) resolution

is of the same order allowing to determine 30-50 independent measurement points in the range 1-4 µm and 15 – 20 in the NIR range.
The third step in the calibration chain is the determination of nonlinearities in the detection circuit. One measures the spectra obtained from a black body source between 150°C and 1250°C at intervals of 100°C. When taking spectra at the same temperature but different exposure times one notices that the exposure times shorter than 1000 µs need to be corrected. In our case we use e.g. 83.2 µs instead 50 µs and 212.4 µs instead of 200 µs. After this correction one finds a polynom (2) with the coefficients A= -20000, B= 0.83, C= $1.9*10^{-9}$ and D= $-0.5*10^{-18}$ that linearises the overall gain for the whole dynamic range and the three wavelengths of particular interest (1.6, 2.0 and 3.6 µm).

$$I_{cor} = A + B \cdot I_{mes} + C \cdot I_{mes}^2 + D \cdot I_{mes}^3 \qquad (2)$$

I_{cor} in (2) corresponds to a value directly proportional to the luminance L_{BB} of a black body radiator (3) of the temperature T (in K) and the wavelength λ (h Planck constant, k_b Boltzmann constant, c speed of light).

$$L_{BB}(l,T) = \frac{2 \cdot h \cdot c}{l^5 \cdot \left(\exp^{\left(\frac{h \cdot c}{l \cdot k_b \cdot T} \right)} - 1 \right)} \qquad (3)$$

knowing the transmission t (λ) of the fibre and the emissivity of the black body radiator (0.98) one can calculate the sensitivity s(λ) of the detector according to equ. 4.

$$I_{cor}(l,T) = t(l) \times s(l) \times e(l,T) \times L_{BB}(l,T) \qquad (4)$$

Fig. 3 gives the sensitivity actually used (t > 0.2ms) and two other ones which are not corrected for the nonlinearities described above. When applying all corrections mentioned above they rejoin the nominal sensitivity curve.
The overall dynamic range of the prism spectrometer without external fibres reaches from 160 to 1050 °C (fig. 4). In our application with transmission in the fibre and periscope arrangement often being less than 10% these values shift upwards to 200 – 1500°C or higher.

4. Data acqusition and treatment

The general features of the data-acquisition system have been described elsewhere [2]. The data analysis automatically performed for each discharge is illustrated in fig. 4. It determines for 1.6 µm, 2 µm and where possible also for 3.6 µm and for all fibres available a temperature by using the linearisation procedures outlined above and lookup tables for all transmission values and the conversion of luminance into temperature. Since only carbonaceaous targets with high emissivity values (0.73 – 0.95) are observed which are usually considerably hotter than the environment, the analysis follows equ. (4) ignoring reflections. Spectra as in fig. 5 can be obtained manually for more precise analysis.

5. Discussion

The overall reliability of the system is very high. After more than 2 years of operation (30% duty cycle) in a total of 3 similar cameras one failure has occurred. The most important

problems encountered were the nonlinearities mentioned above in the calibration section and changes in the overall transmission of the fibres following water leaks inside the torus. This damage seems to be permanent for the hygroscopic ZrF_4 fibres. Less important were effects from gradual deposit accumulation on the sapphire of the periscopes. The degradation of the transmission required considerable in vessel calibration effort. The optical performance of the system are as predicted by the design. The spectral analysis had been useful to verify the transmission data for the IR fibres of the various fibre manufacturer. When comparing the temperature data obtained by this prism spectrometer with another system working in the near infrared range [7], one finds good agreement within ±10%.
The potential of this approach of measuring a whole spectrum and not only at one wavelength is illustrated in fig. 6. It shows luminance distributions synthetised using a weighted sum of black body luminances of 8 discrete temperatures T_n (‘test fraction‘ in fig. 6) reconstituted by 3 weighted sums (‘fit fraction‘ in fig. 6) of black body luminances at the temperatures T_m by using a least square approximation (equ.5). The fitted luminances are indistinguishable from the original ones in fig. 6. The fit values reproduce in all three cases the main features of the test fraction: either a large homogeneous distribution or a wide gaussian shape or a double distribution with a small fraction of a hot contribution.

$$\sum_{n=1}^{8} L_{BB}(l, T_n) \cdot f_n = \sum_{m=1}^{3} L_{BB}(l, T_m) \cdot f_m \qquad (5)$$

7. Conclusion

The diagnostic works well and performs up to expectations. The data analysis presently supplies multi spectral multi temperature data but does not yet exploit the full potential of the system. This potential is to able to determine the main features of a temperature distribution as encountered in relevant tokamak conditions from a spectrally resolved observation. Applied to ITER this may allow an interesting trade off between spatial and spectral resolution. On the strength of this concept and in view of encouraging radiation hardness data in particular concerning silica fibres [10, 11], one can consider a similar concept for ITER which may have also interesting calibration possibilities by laser light transmitted to the target. More work is needed for radiation hard IR fibres.

References:

[1] D. Guilhem et al., Rev. Sci. Instr. **70** (1999) 427-430
[2] R. Reichle et al., Nucl. Fusion **43** (2003) 797-804
[3] Garin, P., Fusion Engineering and Design, **49-50** (2000) 89
[4] Delchambre, E., et al, proc. 30th EPS Contr. Fusion and Plasma Physics, (St. Petersburg, Russia, 7-11 July 2003), ECA **27A**, P3.169 (2003).
[5] Vallet, J.C. et al., proc. 30th EPS Contr. Fusion and Plasma Physics, (St. Petersburg, Russia, 7-11 July 2003), ECA **27A**, P1.137 (2003).
[6] Reichle, R., et al., contrib. 10th Carbon Workshop Juelich, Germany, 16 – 19 Sept 2003, accepted for publication in Physica Scripta
[7] Reichle, R. et al., J. Nucl. Mater., **290-293** (2001) 701
[8] Reichle, R., et al., J. Nucl. Mater., **313-316** (2003) 711
[9] Delchambre, E., et al, proc. 30th EPS Contr. Fusion and Plasma Physics, (St. Petersburg, Russia, 7-11 July 2003), ECA **27A**, P1.068 (2003).
[10] Herrmann, A., et al., contrib. 10th Carbon Workshop Juelich, Germany, 16 – 19 Sept 2003, accepted for publication in Physica Scripta
[10] Shikama, T., et al. Nucl. Instr. Meth. In Phys Res., **B91** (1994) 342
[11] Brichard, B., et al, Fusion Engineering and Design, **56-57**(2001) 917-921

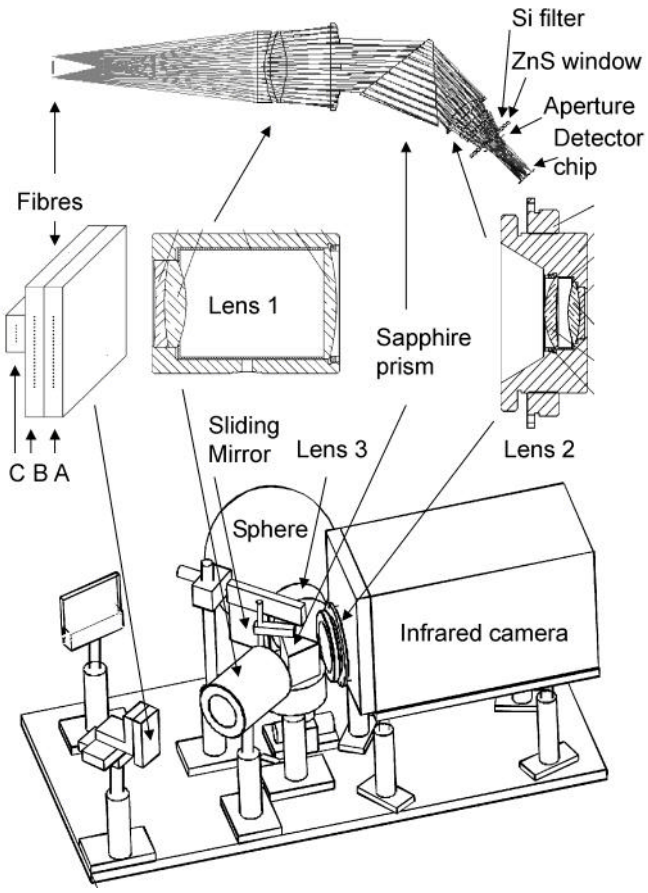

Fig. 1: Overview of set-up.

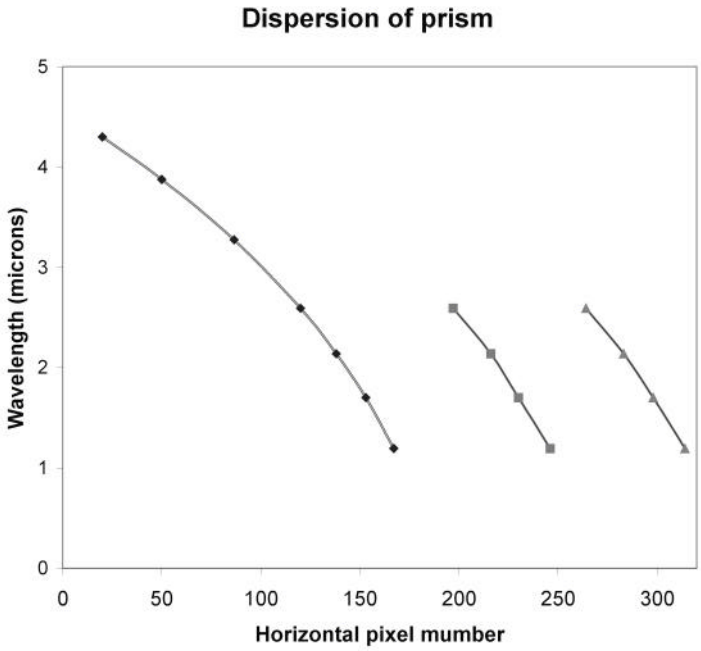

Fig. 2: Dispersion curves of prism.

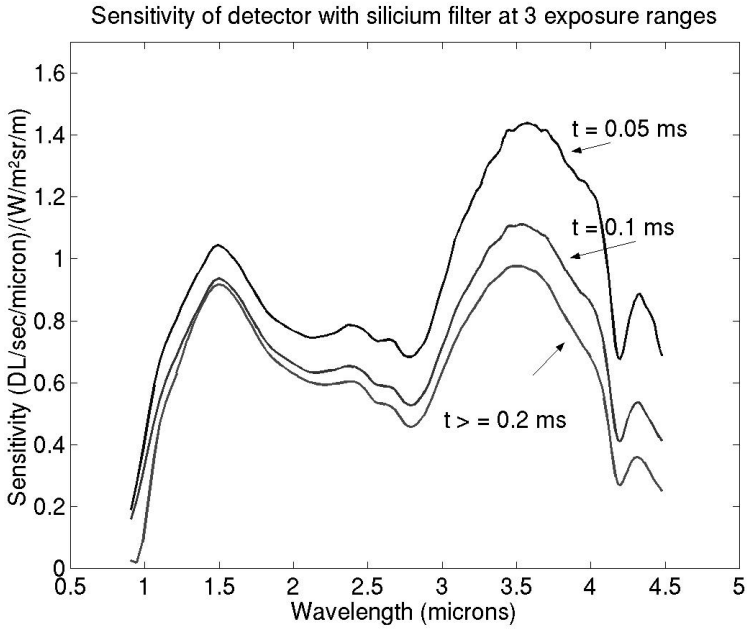

Fig. 3: Sensitivity of InSb detector.

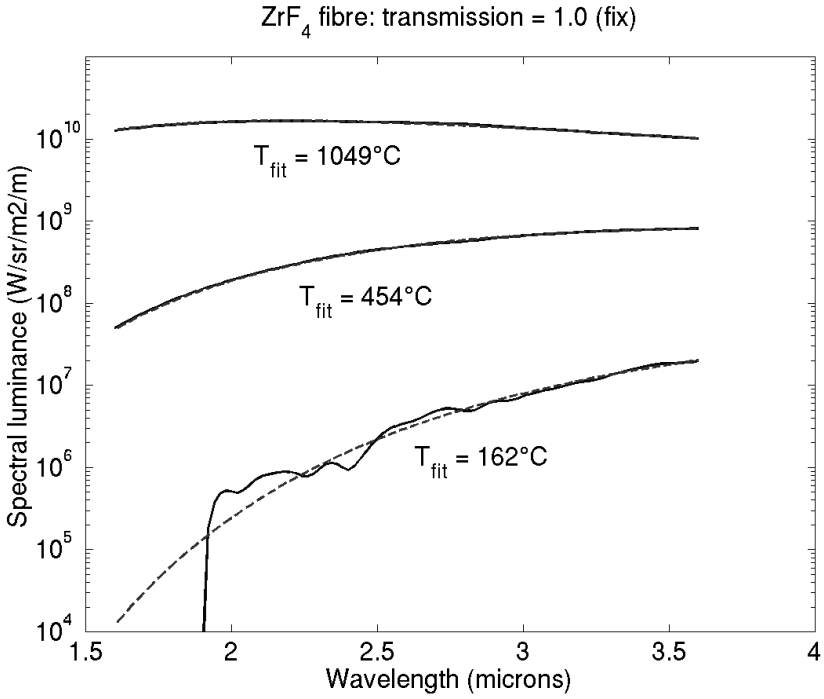

Fig. 4: Comparison of measured and calculated black body spectra.

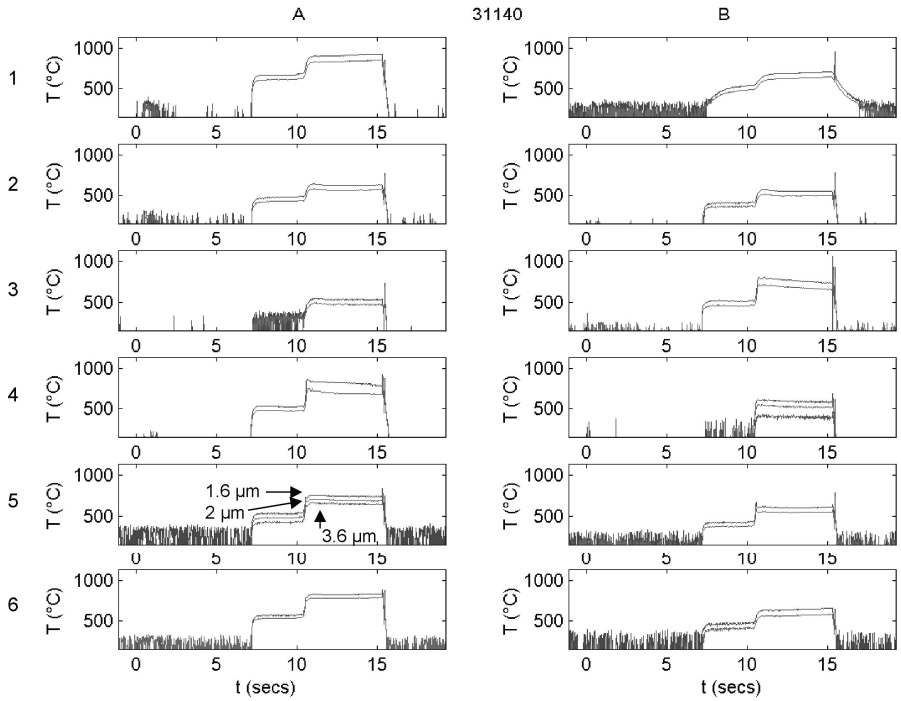

Fig. 5: Example of temporal traces of processed data during a discharge.

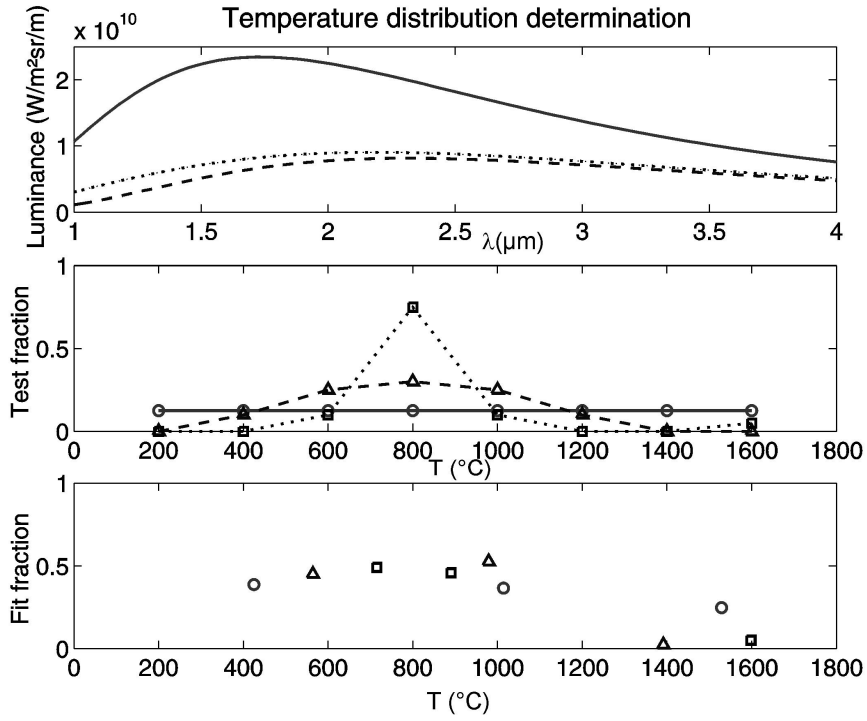

Fig. 6: 3 Luminance distributions produced by weighted distributions of 8 and 3 temperatures. (continuos line and circles: flat distribution; dashed line and triangles: large gaussian distribution; dotted line and squares: narrow distribution with additional small high temperature fraction).